DOI: 10.48011/asba.v2i1.1396

Modeling and Control of Four-bar Mechanism with Series Elastic Actuators ⋆

Felipe R. Lopes * **Marco A. Meggiolaro** *

* *Mechanical Engineering Department, Pontifical Catholic University of Rio de Janeiro, RJ, (e-mail: felipelopes_9@hotmail.com).*

Abstract: A new generation of robots that work in cooperation with humans (called collaborative robots) needs some flexibility to adapt to the environment and activities with people. That is why the Series Elastic Actuator (SEA) has been a breakthrough in actuator technologies. The idea of inserting an elastic element in series with a motor allows a lower output impedance, consequently a flexible behavior in the manipulator, in addition to providing torque feedback to better compensate disturbances caused e.g. by friction losses. This article presents a four-bar mechanism with SEA for the purpose of robotic manipulation. Its kinematics and dynamics are studied, as well as its regulation and trajectory control. The behavior of the decoupled four-bar mechanism and the characteristics of the SEA are also analyzed. Then the regulation control of the complete system is carried out using LQR control. Finally, a circular trajectory is controlled in a simulation to validate the proposed control strategy. The simulation results show the effectiveness of the proposed controller for the mechanism in the presence of SEAs estimating torque and providing the desired compliance for human interaction.

Keywords: Robot Control, Human-Robot Interaction, Series Elastic Actuator, Four-Bar Mechanism, Linear Control

1. INTRODUCTION

Safety is one of the main topics for robots to be able to work collaboratively in activities with human beings. This involves refined force control in robotic systems, requiring more accurate but more expensive force sensors. The Series Elastic Actuator (SEA) has proven to be a low cost and high potential improvement used not only in industrial robots, but also in many research robots.

The SEA adds flexibility through an elastic element connected between the motor side and the link side. It allows better force/torque control, low impedance, and impact tolerance on the motor side. This type of performance has been widely used in mechatronic applications, especially in humanoid robots.

This form of mechanical compliance guarantees an inertial decoupling between the actuator and the driven robot link, thus reducing the kinetic energy involved in undesired collisions with humans. Also, the motor and disturbance torques become physically collocated, an important characteristic for the rejection of vibrations (De Luca and Book, 2016). However, the hysteresis of the spring element may cause relevant inaccuracy in the SEA measurement.

Despite these difficulties, several SEA applications – e.g. for quadruped robots, biped robot, dual-arm robots, and wearable robots – have demonstrated that it is a promising actuator system. (Lee et al., 2017)

Several examples of systems that use SEA can be found in the literature, mainly in areas such as Rehabilitation Robots (Chen et al., 2019; DeBoon et al., 2019; Miyata and Ahmadi, 2019; Lee et al., 2018), and Exoskeletons and Prostheses (Alamdari et al., 2019; Bianchi et al., 2018; Chen et al., 2019; Convens et al., 2019; Freitas et al., 2019; Woo et al., 2017). Other major areas where this type of actuator can also be found are in the study of locomotion of robotic platforms (Knabe et al., 2015; Lee and Oh, 2019; Ruppert and Sprowitz, 2019; Schumann et al., 2019; Zhang et al., 2019), and in Physical Human-Robot Interaction (pHRI) (Lee et al., 2019; Shi et al., 2020).

In Shi et al. (2020) for example, SEA was used with a collision detection algorithm to work safely with both humans and plants. The article proposed a method to describe the magnitude and position of the impact that occurs on the manipulator while it performs the picking process.

There are several physical implementations of the elements that connect the motor and the link, as discussed in (Lin et al., 2017; Leal-Junior et al., 2018; Cummings et al., 2016), where a rigid element with specific geometry can achieve the desired deflection. In Cappello et al. (2019), e.g., a compliant element with multiple equilibrium positions is presented for use in assistive robotics. In addition to these, Jarrett and McDaid (2019); Kim and Oh (2019); Kakogawa and Ma (2018) feature elastomers performing the spring function.

Some well-known dual-arm robots that use the SEA should also be mentioned, namely the Valkyrie robot (Radford

⋆ This study was financed in part by FAPERJ and the Coordenação de Aperfeiçoamento de Pessoal de Nível Superior - Brasil (CAPES) - Finance Code 001.

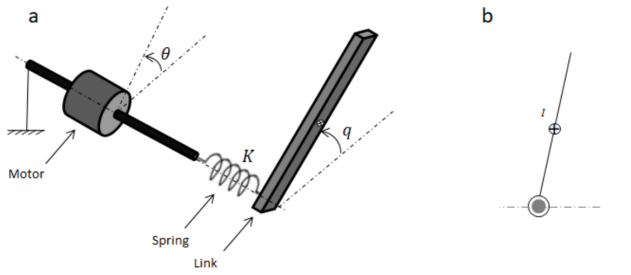

Figure 1. Series Elastic Actuator. a) One-Link SEA model. b) SEA 2D Representation

et al., 2015) and the Baxter Robot (Guizzo and Ackerman, 2012).

This work presents the modeling of a 4-bar mechanism that uses a series elastic actuator for robotic manipulation, as well as its regulation and trajectory control using full state feedback. The 4-bar mechanism features a closed kinematic chain that allows it to perform 2D trajectories with two degrees of freedom (DOF), with both drive motors placed on the robot base. It is widely used in several industrial applications due to lower cost, higher precision when following a particular trajectory, greater force rates, and simplicity compared to serial mechanisms due to the simpler motor placement (for the first joints) on the base instead of the links. (Rodríguez-Molina et al., 2019).

2. SERIES ELASTIC ACTUATOR PRINCIPLES

Pratt and Williamson (1995) introduced the SEA concept, which was later detailed by Pratt et al. (2002), where possible applications for the actuator are described. A precise analysis of the three types of SEA was made in Paine et al. (2013) and Lee et al. (2017), where they compare each category with respect to force sensitivity, compliance and transmissibility.

A schematic is represented in Fig.1, where the position of the motor axis (θ) and the link position (q) are considered as measured quantities, the spring elastic constant is K, and the output force F can be calculated by Hooke's law:

$$F = K(\theta - q) \tag{1}$$

Let's assume small deformations and therefore a linear elastic behavior of the SEA system. Based on Fig.1, one can write the dynamic equation for a link with SEA in the form:

$$I\ddot{q} + mgl sin(q) + K_s(q - \theta) = 0 \tag{2}$$

$$J\ddot{\theta} + B\dot{\theta} + K_s(\theta - q) = \tau \tag{3}$$

where I, m and l correspond to the inertia, mass, and length of the link, respectively, J and B are the motor inertia and friction coefficient, g is gravity acceleration, and τ is the motor torque.

Note that the systems are coupled by the term $K(\theta - q)$, while the actuation occurs only on the motors. The torque is then transmitted by the elastic element and thus induces the movement on the link. In the next section, the

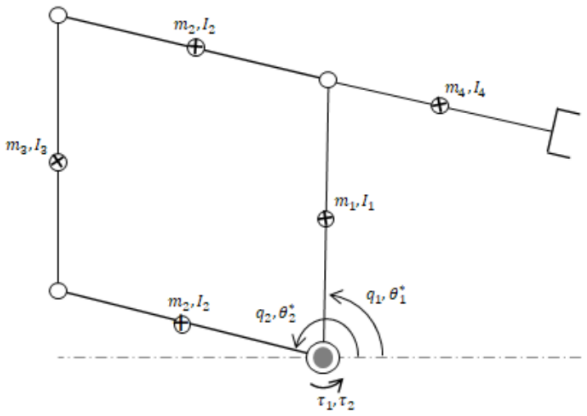

Figure 2. Planar Four-Bar Mechanism

dynamics of the considered 4-bar mechanism manipulator is developed, to be used along with the SEA model.

3. DYNAMICS OF FOUR-BAR MECHANISM WITH SEA

At first, the mechanism is modeled with rigid connections between links and their drive motors. The model is represented by Fig.2.

The manipulator acts on the XY Cartesian plane and the coordinates of the end effector are given by:

$$x = l_1.cos(q_1) - l_4.cos(q_2) \tag{4}$$

$$y = l_1.sin(q_1) - l_4.sin(q_2) \tag{5}$$

where l_1 and l_4 are the lengths of links 1 and 4, respectively, and q_1 and q_2 are the link angles with respect to the horizontal (using absolute coordinates).

The Jacobian of the manipulator, which relates the joint velocities to the end-effector velocities, is given by:

$$J = \begin{bmatrix} -l_1.sin(q_1) & l_4.sin(q_2) \\ l_1.cos(q_1) & -l_4.cos(q_2) \end{bmatrix} \tag{6}$$

Following the Lagrangian approach, the energy contributions are:

$$L = T(q, \dot{q}) - U(q) \tag{7}$$

where $T(q, \dot{q})$ and $U(q)$ are respectively the kinetic and potential energies, and q the joint position vector $[q_1 \quad q_2]^T$. The kinetic energy is calculated by:

$$T = \frac{1}{2}\sum_{i=1}^{n} m_i|v_{ci}|^2 + I_i|w_i|^2 \tag{8}$$

where n is the number of links, m_i, v_{ci}, I_i e ω_i are the mass, linear velocity of the center of mass, moment of inertia with respect to the center of mass, and angular velocity of the i-th link, respectively.

To calculate the kinetic energy, all linear and angular velocities of the center of mass of the links are computed:

$$v_{c1} = \begin{bmatrix} l_{c1}.sin(q_1) & 0 \\ l_{c1}.cos(q_1) & 0 \end{bmatrix} \cdot \begin{bmatrix} \dot{q}_1 \\ \dot{q}_2 \end{bmatrix} \quad (9)$$

$$v_{c2} = \begin{bmatrix} 0 & l_{c2}.sin(q_2) \\ 0 & l_{c2}.cos(q_2) \end{bmatrix} \cdot \begin{bmatrix} \dot{q}_1 \\ \dot{q}_2 \end{bmatrix} \quad (10)$$

$$v_{c3} = \begin{bmatrix} -l_{c3}.sin(q_1) & -l_2.sin(q_2) \\ l_{c3}.cos(q_1) & l_2.cos(q_2) \end{bmatrix} \cdot \begin{bmatrix} \dot{q}_1 \\ \dot{q}_2 \end{bmatrix} \quad (11)$$

$$v_{c4} = \begin{bmatrix} -l_1.sin(q_1) & l_{c4}.sin(q_2) \\ l_1.cos(q_1) & -l_{c4}.cos(q_2) \end{bmatrix} \cdot \begin{bmatrix} \dot{q}_1 \\ \dot{q}_2 \end{bmatrix} \quad (12)$$

$$\begin{bmatrix} w_1 \\ w_2 \\ w_3 \\ w_4 \end{bmatrix} = \begin{bmatrix} 1 & 0 \\ 0 & 1 \\ 1 & 0 \\ 0 & 1 \end{bmatrix} \cdot \begin{bmatrix} \dot{q}_1 \\ \dot{q}_2 \end{bmatrix} \quad (13)$$

Equation (8) can be written as:

$$T = \frac{1}{2}\dot{q}^T H \dot{q} \quad (14)$$

where H is the manipulator inertia matrix. This positive-definite matrix contains the main inertia characteristics of the manipulator, resulting in:

$$H = \begin{bmatrix} H_{11} & H_{12} \\ H_{21} & H_{22} \end{bmatrix} \quad (15)$$

Where:

$$H_{11} = m_1 l_{c1}^2 + m_3 l_{c3}^2 + m_4 l_1^2 + I_1 + I_3 \quad (16)$$

$$H_{22} = m_2 l_{c2}^2 + m_3 l_2^2 + m_4 l_{c4}^2 + I_2 + I_4 \quad (17)$$

$$H_{12} = H_{21} = (m_3 l_2 l_{c3} - m_4 l_1 l_{c4}) cos(q_1 - q_2) \quad (18)$$

From the manipulator inertia matrix, it is possible to calculate terms directly related to centrifugal and Coriolis effects:

$$C = \begin{bmatrix} h_{122} = (m_3 l_2 l_{c3} - m_4 l_1 l_{c4}) sin(q_1 - q_2) \\ h_{211} = -(m_3 l_2 l_{c3} - m_4 l_1 l_{c4}) sin(q_1 - q_2) \end{bmatrix} \quad (19)$$

Since the manipulator is assumed to work on an horizontal plane, gravity effects can be neglected. Thus the potential energy term only needs to consider the SEA elastic potential

$$U_e = \frac{1}{2}(q - \theta)^T K (q - \theta) \quad (20)$$

Where $K = diag(K_1, K_2)$ is a diagonal matrix with elements equal to the stiffness K_i of the SEA from each joint (i = 1, 2).

From the previous equations, it is possible to obtain the equations of motion from the Lagrangian approach:

$$\lambda_1 \ddot{q}_1 + \sigma c_{12} \ddot{q}_2 + \sigma s_{12} \dot{q}_2^2 + K_s(q_1 - \theta_1) = 0 \quad (21)$$

$$\sigma c_{12} \ddot{q}_1 + \lambda_2 \ddot{q}_2 - \sigma s_{12} \dot{q}_1^2 + K_s(q_2 - \theta_2) = 0 \quad (22)$$

$$J_1 \ddot{\theta}_1 + B_1 \dot{\theta}_1 + K_s(\theta_1 - q_1) = \tau_1 \quad (23)$$

$$J_2 \ddot{\theta}_2 + B_2 \dot{\theta}_2 + K_s(\theta_2 - q_2) = \tau_2 \quad (24)$$

Where:

$$\lambda_1 = m_4 l_1^2 + m_1 l_{c1}^2 + m_3 l_{c3}^2 + I_1 + I_3$$
$$\lambda_2 = m_3 l_2^2 + m_2 l_{c2}^2 + m_4 l_{c4}^2 + I_2 + I_4$$
$$\sigma = m_3 l_2 l_{c3} - m_4 l_1 l_{c4}$$
$$c_{12} = cos(q_1 - q_2)$$
$$s_{12} = sin(q_1 - q_2)$$

As seen in Eqs. (21)-(24), there are twice as many generalized coordinates compared to the 4-bar mechanism with rigid motor couplings, to accommodate the compliances of each of the two SEAs. For state feedback this will require the use of 4 position sensors instead of the usual 2 from the rigid version. In addition, note that no Coriolis terms are present, only centrifugal acceleration terms.

4. LINEAR SYSTEM ANALYSIS - DECOUPLED MECHANISM

One way to linearize this system is making the coupling terms of matrix H to be null, forcing $\sigma = 0$ in any configuration. This can be done in the design phase by assuring that:

$$\frac{m_3}{m_4} = \frac{l_1 l_{c4}}{l_2 l_{c3}} \quad (25)$$

Therefore, Eqs. (21)-(22) become:

$$\lambda_1 \ddot{q}_1 + K_s(q_1 - \theta_1) = 0 \quad (26)$$

$$\lambda_2 \ddot{q}_2 + K_s(q_2 - \theta_2) = 0 \quad (27)$$

which can be represented in linear form in a space state representation:

$$\dot{x} = Ax + Bu \quad (28)$$

$$y = Cx + Du \quad (29)$$

$$x = \begin{bmatrix} \theta_1 & \dot{\theta}_1 & q_1 & \dot{q}_1 & \theta_2 & \dot{\theta}_2 & q_2 & \dot{q}_2 \end{bmatrix}^T \quad (30)$$

The state matrix (A) of the resulting linearized and decoupled manipulator is:

$$A = \begin{bmatrix} A1 & 0_{4x4} \\ 0_{4x4} & A2 \end{bmatrix} \quad (31)$$

Where:

$$A1 = \begin{bmatrix} 0 & 1 & 0 & 0 \\ -\frac{K_s}{J_1} & -\frac{(B_1 + B_s)}{J_1} & \frac{K_s}{J_1} & \frac{B_s}{J_1} \\ 0 & 0 & 0 & 1 \\ \frac{K_s}{\lambda_1} & 0 & -\frac{K_s}{\lambda_1} & 0 \end{bmatrix} \quad (32)$$

$$A2 = \begin{bmatrix} 0 & 1 & 0 & 0 \\ -\frac{K_s}{J_2} & -\frac{(B_2 + B_s)}{J_2} & \frac{K_s}{J_2} & \frac{B_s}{J_2} \\ 0 & 0 & 0 & 1 \\ \frac{K_s}{\lambda_2} & 0 & -\frac{K_s}{\lambda_2} & 0 \end{bmatrix} \quad (33)$$

$$B = \begin{bmatrix} 0 & 0 \\ \frac{1}{J_1} & 0 \\ 0 & 0 \\ 0 & 0 \\ 0 & 0 \\ 0 & \frac{1}{J_2} \\ 0 & 0 \\ 0 & 0 \end{bmatrix} \tag{34}$$

$$C = \begin{bmatrix} 1 & 0 & 0 & 0 & 0 & 0 & 0 & 0 \\ 0 & 0 & 1 & 0 & 0 & 0 & 0 & 0 \\ 0 & 0 & 0 & 0 & 1 & 0 & 0 & 0 \\ 0 & 0 & 0 & 0 & 0 & 0 & 1 & 0 \end{bmatrix} \tag{35}$$

Also, for the control project, it is necessary to know whether the system is fully controllable. It means that the system can have its poles allocated in the desired positions to make the system stable and meet performance specifications.

Knowing that the closed-loop poles of the system are equivalent to the eigenvalues of state matrix A, it is possible to calculate the system control matrix from:

$$P_c = [B \quad AB \quad A^2B \quad \dots \quad A^{n-1}B] \tag{36}$$

where $n = 8$ is the order of the system. Since the resulting P_c matrix is full rank, the system is completely controlable.

5. SIMULATION

The motor parameters used in the simulations are shown in Table 1. Table 2 shows the adopted manipulator parameters.

Table 1. Motors and Springs Parameters

Element	Value	Unit
K_s	0.48	Nm/rad
J_1	3.7e-3	kg.m^2
J_2	3.7e-3	kg.m^2
B_1	4.6e-2	Nm/m/s
B_2	4.6e-2	Nm/m/s

Table 2. Manipulator Parameters

Element	Value	Unit
l_1	160e-3	m
l_2	160e-3	m
l_3	160e-3	m
l_4	140e-3	m
I_1	5.0213e-4	kg.m^2
I_2	5.0213e-4	kg.m^2
I_3	5.0213e-4	kg.m^2
I_4	4.3937e-4	kg.m^2
m_1	235.4e-3	kg
m_2	235.4e-3	kg
m_3	235.4e-3	kg
m_4	269e-3	kg

Figure 3 presents the root locus of the four-bar system with the two SEAs. The transfer functions θ_1/τ_1 and θ_2/τ_2 are stable, as expected for a collocated system. For the root locus of q_1/τ_1 and q_2/τ_2, as the gain value is increased the system becomes unstable, as expected for a non-collocated system with significant compliance between the sensor and actuator (the SEA compliance).

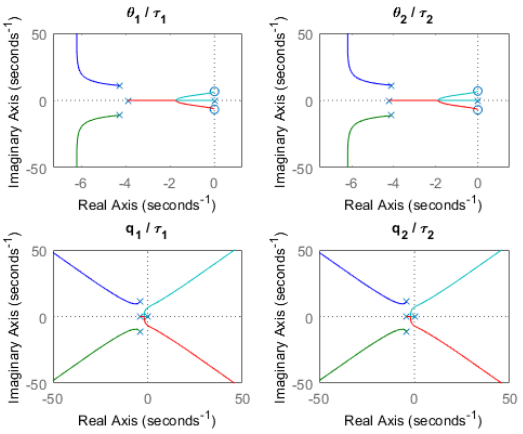

Figure 3. Root Locus of Four-Bar System with SEA

5.1 Regulation Control

In this section, results are presented for the position control of the manipulator to a constant desired configuration. For the initial and desired configurations, the following values are assumed:

$$\Theta_{initial} = \begin{bmatrix} \theta_1 \\ q_1 \\ \theta_2 \\ q_2 \end{bmatrix} = \begin{bmatrix} \pi/2 \\ \pi/2 \\ \pi \\ \pi \end{bmatrix} \tag{37}$$

$$\Theta_{desired} = \begin{bmatrix} \theta_1 \\ q_1 \\ \theta_2 \\ q_2 \end{bmatrix} = \begin{bmatrix} 3\pi/4 \\ 3\pi/4 \\ 5\pi/4 \\ 5\pi/4 \end{bmatrix} \tag{38}$$

Full state feedback is assumed in this work, made possible by 4 encoders to estimate the motors and links positions together with predictive observers to estimate the corresponding velocities, resulting in the linear control law:

$$u(t) := -K.x(t) \tag{39}$$

where K is the gain matrix and x the state vector.

To calculate the feedback gains K it is possible to use the pole allocation method, where the designer chooses the poles to obtain the desired performance. In cases with many states this technique becomes laborious to obtain a desired performance.

Alternatively, an optimal control design can be conducted, aiming to minimize a performance index. Considering the system equation and control law, the LQR control theory aims to minimize

$$J = \int_0^\infty (x^T Q x + u^T R u) dt \tag{40}$$

where Q and R are positive-definite symmetric real matrices that determines the relative importance (weight) of the state error and of the control effort (Ogata, 2011).

To calculate an optimal feedback matrix K, it is necessary to solve the Riccatti equation for a positive-definite matrix P:

$$A^T P + PA - PRB^{-1}B^T P + Q = 0 \tag{41}$$

and then the K gains are calculated by:

$$K = R^{-1}B^T P \tag{42}$$

For the considered 4-bar system the following weight matrices are (arbitrarily) adopted, aiming to minimize position errors, from which K is obtained:

$$Q = diag([0.2 \quad 0 \quad 10 \quad 0 \quad 0.2 \quad 0 \quad 10 \quad 0]) \tag{43}$$
$$R = diag([0.4 \quad 0.4]) \tag{44}$$

$$K^T = \begin{bmatrix} 1.0033 & 0 \\ 0.0021 & 0 \\ 4.0465 & 0 \\ 1.4310 & 0 \\ 0 & 1.0215 \\ 0 & 0.0022 \\ 0 & 4.0282 \\ 0 & 1.3670 \end{bmatrix} \tag{45}$$

Note that the weights from matrix Q that penalize the states of the links were chosen much greater than the elements that penalize the states of the motors (i.e. $10 >> 0.2$), since a precise link control is our main goal, regardless of the required motor oscillations.

Figure 4 shows the step response for the position control of the system using the above calibrated gain matrix K. Note how the link angles (q_1 and q_2) are successfully controlled with little overshoot, while the motor angles (θ_1 and θ_2) suffer high-oscillations needed to control such links. This is an expected behavior of systems with SEAs due to their high compliance, as verified in Camino and Fioravanti (2018).

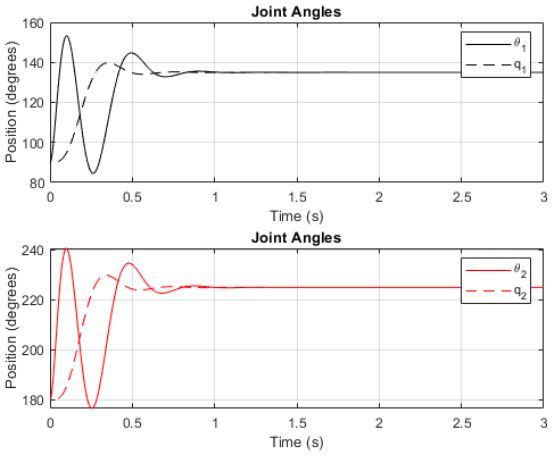

Figure 4. Regulation Control for Joint Positions

The differences $(q_1 - \theta_1)$ and $(q_2 - \theta_2)$ between the link and motor angles depend on the SEA elastic element between them: the higher the stiffness, the lower the difference. If the SEA stiffness is extremely high, then each joint behaves as a rigid body.

5.2 Trajectory Control

For trajectory control, it is necessary to calculate the inverse kinematics of the manipulator. This is because the trajectory is given in the end-effector space, while joint control requires the positions (and velocities) of the manipulator joints.

Using trigonometric relations and observing Fig. 5, it is possible to arrive at the inverse kinematics equations:

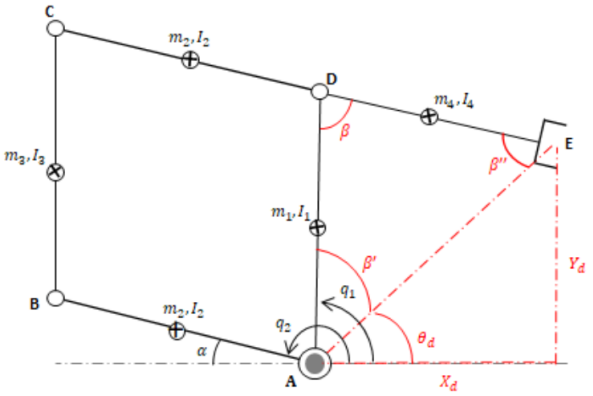

Figure 5. Inverse Kinematics

$$q_1 = \beta' + \theta_d \tag{46}$$
$$q_2 = \theta_d + \beta + \beta' \tag{47}$$

Where:

$$\overline{AE} = \sqrt{(y_d^2 + x_d^2)}$$
$$\theta_d = tan^{-1}\left(\frac{y_d}{x_d}\right)$$
$$\beta = cos^{-1}\left(\frac{l_1^2 + l_4^2 - \overline{AE}^2}{2.l_1.l_4}\right)$$
$$\beta' = sin^{-1}\left(\frac{l_4}{\overline{AE}}.sin(\beta)\right)$$

The desired end-effector path is a circumference of radius 50mm, tracked using the same control law as before.

Figure 6 depicts the manipulator and its end-effector trajectory. Figure 7 shows the desired (dashed line) and actual (solid line) end-effector trajectories. It is possible to see that the manipulator was able to carry out the trajectory with errors of at most 1 mm, except during its initial depart from the circumference center.

It is worth considering that, in order not to saturate the motor, the feedback gain K was adjusted using LQR (through the weight matrix R) so that the maximum motor torque during this trajectory is between ± 2 Nm,

which is the saturation limit of the motors that will be used, in future work, to build the experimental system. As confirmed in Fig. 8, both motors do not exceed this range.

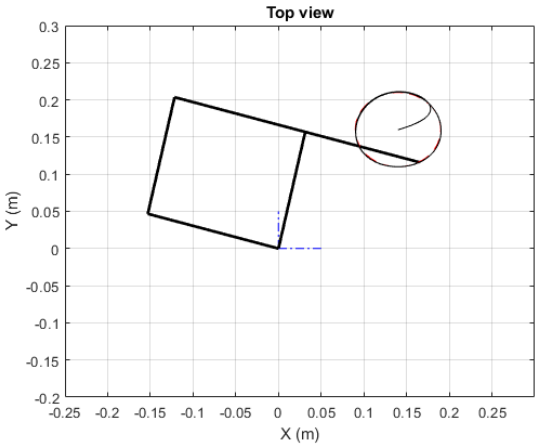

Figure 6. Four-bar Mechanism with SEA Performing a Circular Trajectory

Figure 7. Desired Circular Trajectory

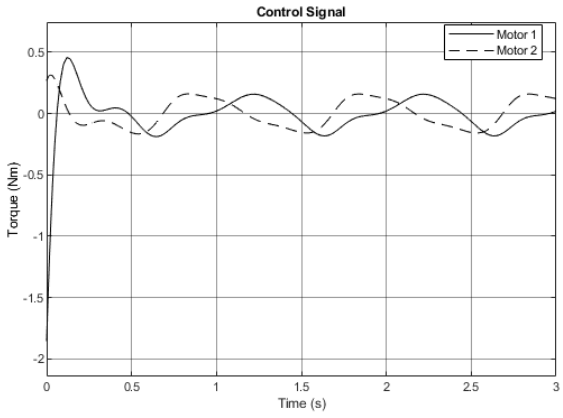

Figure 8. Control Signal of Four-Bar Mechanism with SEA

6. CONCLUSION

In this paper, the kinematics and dynamics of a 4-bar mechanism with series elastic actuators (SEAs) were obtained and an *LQR* control was used for trajectory control along a circular path. Numerical simulations were performed, showing that position errors converged to zero less than 1s for a step response of $\pi/4$ in all joints. As in any system with flexible elements, control gain calibration to ensure performance and stability are a greater challenge. The presented design and control strategy will be used in future works in a system consisting of two independent manipulators working on a coordinated task involving internal forces.

ACKNOWLEDGMENTS

The authors would like to thank the Brazilian agency FAPERJ for its financial support. This study was financed in part by the Coordenação de Aperfeiçoamento de Pessoal de Nível Superior - Brasil (CAPES) - Finance Code 001.

REFERENCES

Alamdari, A., Haghighi, R., and Krovi, V. (2019). Gravity-balancing of elastic articulated-cable leg-orthosis emulator. *Mechanism and machine theory*, 131, 351–370.

Bianchi, M., Cempini, M., Conti, R., Meli, E., Ridolfi, A., Vitiello, N., and Allotta, B. (2018). Design of a series elastic transmission for hand exoskeletons. *Mechatronics*, 51, 8–18.

Camino, J.F. and Fioravanti, A. (2018). Control of a single-link flexible-joint robot via backstepping. In *XXII Congresso Brasileiro de Automática, Joao Pessoa, Sept.*

Cappello, L., Xiloyannis, M., Dinh, B.K., Pirrera, A., Mattioni, F., and Masia, L. (2019). Multistable series elastic actuators: Design and control. *Robotics and Autonomous Systems*, 118, 167–178.

Chen, S., Zhao, J., and Yu, Z. (2019). Adaptive sliding control for lower exoskeleton robot driven by the series elastic actuator. In *2019 IEEE International Conference on Mechatronics and Automation (ICMA)*, 2439–2444. IEEE.

Convens, B., Dong, D., Furnémont, R., Verstraten, T., Cherelle, P., Lefeber, D., and Vanderborght, B. (2019). Modeling, design and test-bench validation of a semi-active propulsive ankle prosthesis with a clutched series elastic actuator. *IEEE Robotics and Automation Letters*, 4(2), 1823–1830.

Cummings, J.P., Ruiken, D., Wilkinson, E.L., Lanighan, M.W., Grupen, R.A., and Sup, F.C. (2016). A compact, modular series elastic actuator. *Journal of Mechanisms and Robotics*, 8(4).

De Luca, A. and Book, W.J. (2016). Robots with flexible elements. In *Springer Handbook of Robotics*, 243–282. Springer.

DeBoon, B., Nokleby, S., La Delfa, N., and Rossa, C. (2019). Differentially-clutched series elastic actuator for robot-aided musculoskeletal rehabilitation. In *2019 International Conference on Robotics and Automation (ICRA)*, 1507–1513. IEEE.

Freitas, B., Silva, M., Carvalho, Ó., Renjewski, D., Fonseca, J., Flores, P., and Espregueira-Mendes, J. (2019). Design, modelling and control of an active weight-bearing knee exoskeleton with a series elastic actuator. In *2019 IEEE 6th Portuguese Meeting on Bioengineering (ENBENG)*, 1–4. IEEE.

Guizzo, E. and Ackerman, E. (2012). How rethink robotics built its new baxter robot worker. *IEEE spectrum*, 7.

Jarrett, C. and McDaid, A. (2019). Modeling and feasibility of an elastomer-based series elastic actuator as a haptic interaction sensor for exoskeleton robotics. *IEEE/ASME Transactions on Mechatronics*, 24(3), 1325–1333.

Kakogawa, A. and Ma, S. (2018). A differential elastic joint for multi-linked pipeline inspection robots. In *2018 IEEE/RSJ International Conference on Intelligent Robots and Systems (IROS)*, 949–954. IEEE.

Kim, D.H. and Oh, J.H. (2019). Hysteresis modeling for torque control of an elastomer series elastic actuator. *IEEE/ASME Transactions on Mechatronics*, 24(3), 1316–1324.

Knabe, C., Seminatore, J., Webb, J., Hopkins, M., Furukawa, T., Leonessa, A., and Lattimer, B. (2015). Design of a series elastic humanoid for the darpa robotics challenge. In *2015 IEEE-RAS 15th International Conference on Humanoid Robots (Humanoids)*, 738–743. IEEE.

Leal-Junior, A.G., Frizera, A., Marques, C., Sánchez, M.R., dos Santos, W.M., Siqueira, A.A., Segatto, M.V., and Pontes, M.J. (2018). Polymer optical fiber for angle and torque measurements of a series elastic actuator's spring. *Journal of Lightwave Technology*, 36(9), 1698–1705.

Lee, C., Cheon, D., and Oh, S. (2019). High fidelity impedance control of series elastic actuator for physical human-machine interaction. In *IECON 2019-45th Annual Conference of the IEEE Industrial Electronics Society*, volume 1, 3621–3626. IEEE.

Lee, C., Kim, J.Y., Kim, S.Y., and Oh, S. (2018). Human force observation and assistance for lower limb rehabilitation using wire-driven series elastic actuator. *Mechatronics*, 55, 13–26.

Lee, C., Kwak, S., Kwak, J., and Oh, S. (2017). Generalization of series elastic actuator configurations and dynamic behavior comparison. In *Actuators*, volume 6, 26.

Lee, C. and Oh, S. (2019). Development, analysis, and control of series elastic actuator-driven robot leg. *Frontiers in neurorobotics*, 13.

Lin, G., Zhao, X., and Han, J. (2017). A novel stiffness control method for series elastic actuator. In *Seventh International Conference on Electronics and Information Engineering*, volume 10322, 103222V. International Society for Optics and Photonics.

Miyata, C. and Ahmadi, M. (2019). Compliant limb sensing and control for safe human-robot interactions. In *2019 International Conference on Robotics and Automation (ICRA)*, 7484–7490. IEEE.

Ogata, K. (2011). Engenharia de controle moderno.5º edição. *Editora LTC*.

Paine, N., Oh, S., and Sentis, L. (2013). Design and control considerations for high-performance series elastic actuators. *IEEE/ASME Transactions on Mechatronics*, 19(3), 1080–1091.

Pratt, G.A. and Williamson, M.M. (1995). Series elastic actuators. In *Proceedings 1995 IEEE/RSJ International Conference on Intelligent Robots and Systems. Human Robot Interaction and Cooperative Robots*, volume 1, 399–406. IEEE.

Pratt, J., Krupp, B., and Morse, C. (2002). Series elastic actuators for high fidelity force control. *Industrial Robot: An International Journal*.

Radford, N.A., Strawser, P., Hambuchen, K., Mehling, J.S., Verdeyen, W.K., Donnan, A.S., Holley, J., Sanchez, J., Nguyen, V., Bridgwater, L., et al. (2015). Valkyrie: Nasa's first bipedal humanoid robot. *Journal of Field Robotics*, 32(3), 397–419.

Rodríguez-Molina, A., Villarreal-Cervantes, M.G., Mezura-Montes, E., and Aldape-Pérez, M. (2019). Adaptive controller tuning method based on online multiobjective optimization: A case study of the four-bar mechanism. *IEEE transactions on cybernetics*.

Ruppert, F. and Sprowitz, A.T. (2019). Series elastic behavior of biarticular muscle-tendon structure in a robotic leg. *Frontiers in neurorobotics*, 13, 64.

Schumann, E., Smit-Anseeuw, N., Zaytsev, P., Gleason, R., Shorter, K.A., and Remy, C.D. (2019). Effects of foot stiffness and damping on walking robot performance. In *2019 International Conference on Robotics and Automation (ICRA)*, 3698–3704. IEEE.

Shi, Y., Zhang, W., Yang, T., Wang, Y., Liu, L., and Cui, Y. (2020). Flexible joints of picking manipulator based on current feedback. *IEEE Access*, 8, 85329–85338.

Woo, H., Na, B., and Kong, K. (2017). Design of a compact rotary series elastic actuator for improved actuation transparency and mechanical safety. In *2017 IEEE International Conference on Robotics and Automation (ICRA)*, 1872–1877. IEEE.

Zhang, Z.Q., Yang, Q., Zhao, J., and Gui, S. (2019). Dynamic model and performance analysis of rigid-flexible coupling four-bar leg mechanism for small scale bio-inspired jumping robot. *Microsystem Technologies*, 25(9), 3269–3285.